ADVANCED MATERIALS
www.afm-journal.de
www.MaterialsViews.com

Quantifying the Energy Barriers and Elucidating the Charge Transport Mechanisms across Interspherulite Boundaries in Solution-Processed Organic Semiconductor Thin Films

*Anna K. Hailey, Szu-Ying Wang, Yuanzhen Chen, Marcia M. Payne, John E. Anthony, Vitaly Podzorov, and Yueh-Lin Loo**

Grain boundaries act as bottlenecks to charge transport in devices comprising polycrystalline organic active layers. To improve device performance, the nature and resulting impact of these boundaries must be better understood. The densities and energy levels of shallow traps within and across triethylsilylethynyl anthradithiophene (TES ADT) spherulites are quantified. The trap density is 7×10^{10} cm^{-2} in devices whose channels reside within a single spherulite and up to 3×10^{11} cm^{-2} for devices whose channels span a spherulite boundary. The activation energy for charge transport, E_A, increases from 34 meV within a spherulite to 50–66 meV across a boundary, depending on the angle of molecular mismatch. Despite being molecular in nature, these E_A's are more akin to those found for charge transport in polymer semiconductors. Presumably, trapped TES ADT at the boundary can electrically connect neighboring spherulites, similar to polymer chains connecting crystallites in polymer semiconductor thin films.

1. Introduction

Organic semiconductors are attracting attention as possible active layers for photovoltaics, transistors, and displays due to their low cost, tunable synthesis, and their amenability to facile processing on flexible substrates. Unfortunately, the rapid deposition methods conducive to high-throughput, large-area device fabrication can leave organic semiconductor thin films kinetically trapped in a polycrystalline state. In these polycrystalline active layers, charge carriers must traverse the boundaries between randomly oriented crystalline grains, which can restrict their mobility. Among computational and theoretical descriptions of charge transport in polycrystalline films, grain boundaries have alternatively been described as charge trapping sites, charge scattering sites, and potential energy barriers.[1] In order to optimize devices based on these polycrystalline active layers, we thus need to improve our understanding of how grain boundaries impact charge transport. However, extracting significant, generalizable results from singular charge transport measurements across polycrystalline films is difficult due to the challenges in controlling structural heterogeneities, such as molecular orientation and grain boundary density, over macroscopic distances. Case in point are the seemingly contradictory experimental studies of charge transport in organic field-effect transistors (OFETs) that show no correlation,[2] negative correlation,[1d,3] and positive correlation,[4] of grain boundary density with room-temperature device mobilities. There are thus gaps in our understanding of how the specifics of these boundaries affect charge transport, as it would be too simplistic to assume that "all boundaries are created equal."

Indeed, the nature, and thus impact, of grain boundaries on charge transport should depend strongly on the chemical structure of the organic semiconductor and the nature of the crystalline domains and domain boundaries that form. At one end of the spectrum are highly conjugated molecular semiconductors, whose strong π–π interactions render the material insoluble and thus necessitate thermal evaporation to form thin films. During thermal evaporation, crystalline grains nucleate and grow as the molecules condense on the substrate. The strong intermolecular interactions force the molecules to adopt a single lattice orientation within each grain, producing well-defined, terraced domains separated by sharp boundaries. It is thus not unreasonable to see voids on the submicrometer length scale at these grain boundaries.[5] While the high crystallinity and order within individual grains is known to facilitate charge transport, these

A. K. Hailey, Prof. Y.-L. Loo
Department of Chemical Engineering
Princeton University
Princeton, NJ 08544, USA
E-mail: lloo@princeton.edu
S.-Y. Wang
Department of Chemistry and Chemical Biology
Rutgers University
Piscataway, NJ 08854, USA
Dr. Y. Chen,[+] Prof. V. Podzorov
Department of Physics and Astronomy
Rutgers University
Piscataway, NJ 08854, USA
Dr. M. M. Payne, Prof. J. E. Anthony
Department of Chemistry
University of Kentucky
Lexington, KY 40506, USA
[+]Present address: Department of Physics, South University of Science and Technology of China, Shenzhen, Guangdong 518055, China

DOI: 10.1002/adfm.201501666

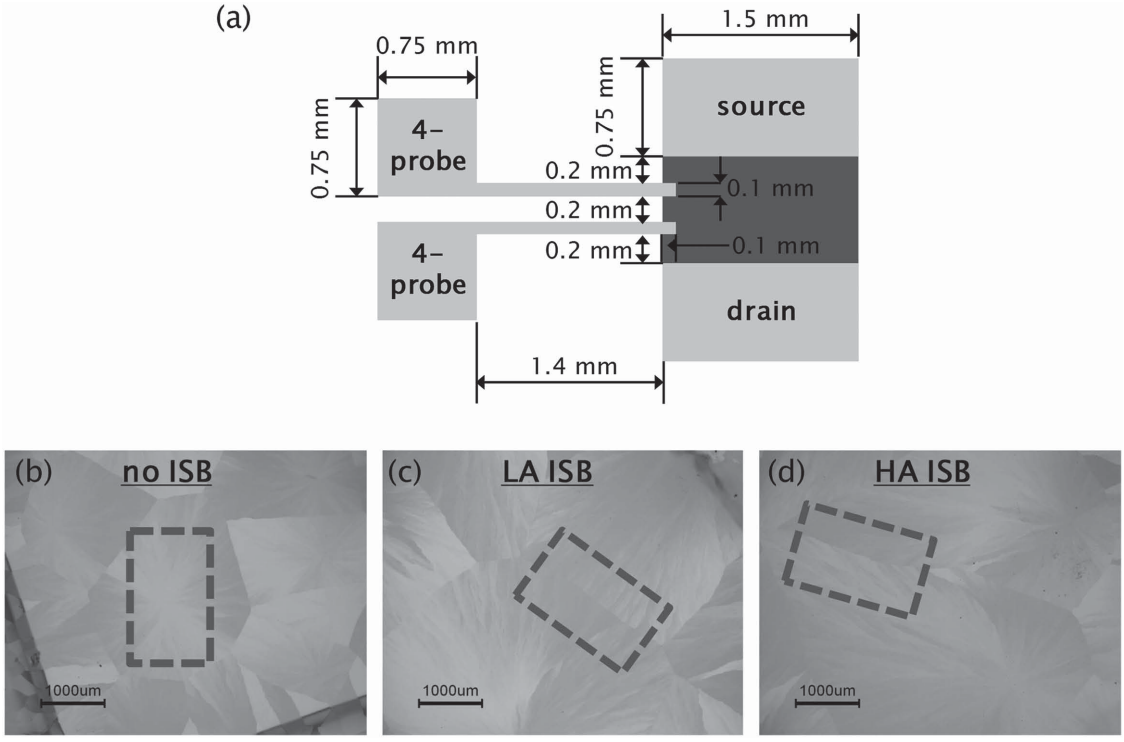

Figure 1. a) Electrode geometry for gated four-probe measurements. The shadow mask was aligned to have an ISB running across the channel between the four-probe voltage electrodes for devices comprising an LA and an HA ISB. The highlighted area in (a) is the active channel of the device. The channel areas of devices b) within a single spherulite (i.e., no ISB), c) comprising an LA ISB, and d) an HA ISB are outlined in the optical micrographs.

perforated boundaries are bottlenecks to macroscopic, intergrain transport. At the other extreme extreme, there are polymeric semiconductors that are highly soluble in common solvents and thus easily solution-processed; deposition from solution often results in a uniform film. During solvent evaporation or subsequent annealing, the long polymer chains crystallize. Different from molecular semiconductors, polymer chains can bridge neighboring crystallites, providing physical connectivity between them. This intercrystallite connectivity is thought to play a critical role in facilitating macroscopic charge transport.[4c,6]

Triethylsilylethynyl anthradithiophene (TES ADT), though a molecular semiconductor, does not form well-defined crystalline grains in the conventional sense. Its bulky triethylsilylethynyl substituents allow the compound to be readily dissolved in common solvents, making it solution-processable. The presence of these substituents also necessarily weakens the π–π interactions between neighboring anthradithiophene cores; spin-coating results in thin films that exhibit limited order but can crystallize to form macroscopic spherulites on subsequent exposure to solvent vapor.[7] These spherulites continue to grow radially outward in the direction of π-stacking until neighboring spherulites impinge. Since these spherulites are four orders of magnitude larger in diameter than in height (1000 μm vs 100 nm, respectively), they are essentially 2D structures. The interspherulite boundaries (ISBs) are thus qualitatively different from those found in conventional molecular-semiconductor thin films or those found in semicrystalline polymeric semiconductor thin films and provide a unique test case for examining charge transport.

2. Results and Discussion

We have classified the ISBs in TES ADT thin films into two categories: low-angle (LA) ISBs refer to those whose angle of molecular mismatch, defined by the two vectors normal to the growth fronts of the impinging spherulites, is 0° ± 20°, and high-angle (HA) ISBs refer to those whose angle of molecular mismatch is 90° ± 20°. We purposefully avoided ISBs with angles of molecular mismatch between these two extremes in order to more distinctly observe the effects of molecular mismatch at the ISBs on charge transport. To measure the impact of ISBs on the current–voltage (I–V) characteristics of TES ADT OFETs, we performed gated four-probe measurements across devices whose active areas span a single LA or HA ISB. For comparison, we also fabricated and tested OFETs whose active areas reside entirely within a single spherulite. Due to the distribution of molecular orientation about the radial axis, however, the active areas of these devices still comprise many LA "intraspherulite" boundaries.[8] Nonetheless, they serve as a reference against which we can measure OFET electrical characteristics that involve interspherulite boundaries. The four-probe geometry (**Figure 1**) allows us to directly measure the channel resistance, thus correcting for contact resistance effects. **Figure 2** shows the I–V curves resulting from three representative devices. With an average threshold voltage (V_T) of –13 ± 2 V, the devices are switched from their on state to their off state as the gate voltage (V_G) is swept from –55 to –5 V, consistent with the hole-transporting nature of charge transport in TES ADT OFETs. As seen in Figure 2, the device constructed within

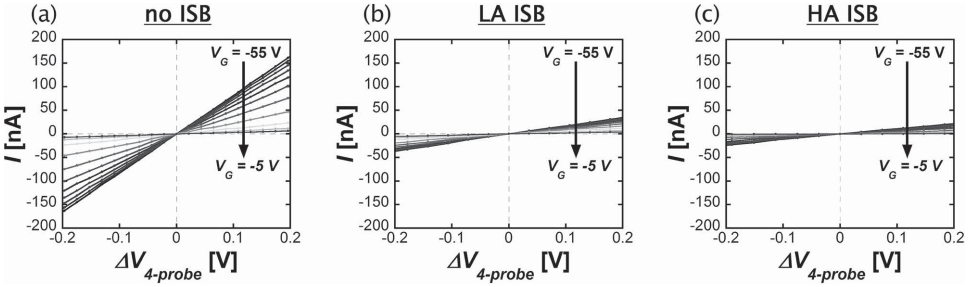

Figure 2. Current–voltage (*I–V*) characteristics obtained from gated four-probe measurements revealing substantial current modulation with the gate voltage (V_G) in a thin-film transistor comprising a) a single spherulite; and current modulations to smaller extents in thin-film transistors comprising b) an LA ISB and c) an HA ISB. Since the average threshold voltage (V_T) of devices was −13 ± 2 V, V_G was swept from −55 to −5 V in +5 V increments corresponding to turning the devices from their fully on to fully off states.

a single TES ADT spherulite exhibits much greater current modulation with gate bias compared to the devices whose channels span either an LA or HA ISB. This result suggests that LA and HA ISBs pose significant barriers to charge transport compared to LA intraspherulite boundaries within individual spherulites.

To elucidate the mechanism of charge transport across ISBs and within spherulites, we performed gated four-probe measurements over a range of temperatures. We observed reproducible behavior down to 215 K for devices whose channels span an ISB and 175 K for devices constructed within individual spherulites. Below these temperatures, TES ADT devices become irreversibly damaged due to cracking of the thin films given the mismatch in thermal expansion coefficients between the TES ADT thin films and the substrate. Interestingly, our observation indicates that devices constructed within single spherulites are less brittle than those spanning ISBs and imply additional mechanical differences introduced by the presence of these boundaries.[9]

We estimated the effective mobility at each V_G in the linear regime per Equation (1)

$$\mu_{\text{eff}} = \left(\frac{L}{WC_{\text{ox}}}\right)\left(\frac{R}{V_G - V_T}\right) \tag{1}$$

where C_{ox} is the capacitance, L and W are the channel length and width, respectively, and R is the channel resistance estimated from the slope of the *I–V* curve.[3a,10] **Figure 3** compiles μ_{eff} as a function of T for devices at a constant carrier concentration, obtained by applying a gate bias 25 V beyond V_T (i.e., $V_G = V_T - 25$ V). Not unlike thin-film transistors comprising other organic semiconductors,[11] our devices display thermally activated mobility (Figure 3). Imposing μ_{eff} as a function of T to both the multiple trap and release (MTR) and the variable range hopping (VRH) models[11,12] has yielded comparable quality of fits over the limited temperature range we can explore. The 1D, 2D, and 3D VRH models, however, predict unreasonable values for the intrinsic mobility (i.e., the mobility in the limit of infinitely high temperature), μ_0, for our devices, ranging from 10^2 to 10^5 cm^2 V^{-1} s^{-1}. If we bound μ_0 to a reasonable limit of 50 cm^2 V^{-1} s^{-1}, the fits to VRH models become very poor. We have thus chosen to use the MTR model, which predicts μ_0 to be ≈10 ± 3 cm^2 V^{-1} s^{-1}, to interpret our results. While μ_0 is often not reported in studies of thermally activated mobility, the μ_0 we calculate for TES ADT devices is consistent with the μ_0 we can determine from data reported for polycrystalline pentacene devices that achieve similarly high contact-corrected mobilities.[13] The MTR model predicts simple thermally activated behavior, described by the Arrhenius equation, for charge hopping to nearest neighbors. In working devices, the energy barrier to charge transport, Δ, decreases with increasing carrier concentration as devices are switched from off to on; Δ saturates at the activation energy, E_A (the minimum, carrier-density independent barrier), when the devices are fully on, as our devices do at $V_G = V_T - 25$ V. This E_A represents the characteristic energy of the exponential distribution of tail states, measured from the highest occupied molecular orbital (HOMO) level for hole transport.[11,12]

To quantify, we calculated the average E_A across three to four devices of each type per Equation (2).

$$\ln\left[\mu_{\text{eff}}(T)|_{V_G - V_T,\text{on}}\right] = -\left(\frac{E_A}{k}\right)\frac{1}{T} + \ln(\mu_0) \tag{2}$$

We found E_A for devices whose channel is within a single spherulite to be 34 ± 3 meV. This energy is only slightly higher than thermal energy at room temperature. Devices whose channels span an LA and HA ISB exhibit E_A of 50 ± 2 and

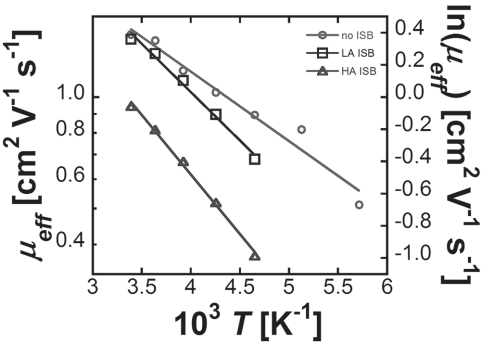

Figure 3. Arrhenius plot of the effective mobilities, μ_{eff}, extracted from gated four-probe variable temperature, T, measurements performed within a single spherulite (circles), across an LA ISB (squares), and across an HA ISB (triangles). All mobilities were extracted at $V_G = V_T - 25$ V, that is, at the same concentration of mobile carriers. The solid lines are the linear fits used to calculate the activation energy, E_A, in each case using Equation (2).

66 ± 1 meV, respectively. Differences in E_A reflect differences in the effective barrier height to charge transport in these devices and suggest that HA ISBs create deeper traps than those associated with LA ISBs.

The activation energies for charge transport, extracted from temperature-dependent mobilities of thin-film transistors comprising polycrystalline active layers, typically range from 20 to 100 meV for all polymeric and molecular semiconductors.[11] Since E_A for charge transport in a thin-film transistor comprising polycrystalline TES ADT would be limited by E_A for charge transport across its HA ISBs, it is satisfying that the activation energies we calculate fall squarely within the common range of values. However, the barrier to charge transport depends on many factors, ranging from the chemical structure and molecular packing to the quality of the dielectric interface and surface preparation.[11] Indeed, Morpurgo and co-workers showed that the temperature dependence of the mobility is strongly correlated with the dielectric constant.[14] Thus, to mitigate any effect that different dielectric layers may have on the charge carriers at the interface, we limited our comparison to those of other devices measured in the linear regime utilizing SiO_2 as the gate dielectric.

Rather than comparing the absolute E_A of TES ADT with those of other molecular or polymeric systems, we can more fairly and usefully compare how much E_A increases with the introduction of boundaries. We have chosen to compare our results, extracted from charge transport across the individual boundaries of TES ADT, with those reported by Frisbie et al., extracted from charge transport across individual boundaries of α-sexithiophene (α-6T).[3a,b,15] An inherent difference between these two materials systems is the fact that TES ADT forms spherulites, whereas α-6T forms well-defined crystalline grains upon thermal evaporation. Yet, since both TES ADT and α-6T pack in 2D motifs (brickwork and herringbone, respectively), and devices comprising these materials exhibit similar intraspherulite (or intragrain in the case of α-6T) hole mobilities of 0.4 and 0.15 $cm^2\ V^{-1}\ s^{-1}$, respectively, we feel that these molecular semiconductors are a relevant comparison.[16] E_A was found to be 40 meV for charge transport within a single-crystalline grain of α-6T, ranging between 55 and 125 meV for charge transport across LA grain boundaries whose angle of molecular mismatch is 8°–13°, and between 128 and 212 meV for charge transport across grain boundaries whose angle of molecular mismatch is 24°–63°.[3a] The increase in E_A with the introduction of grain boundaries in α-6T is much steeper than what we observe in TES ADT. Given differences in the crystalline domains and their boundaries, we surmise this much steeper increase in E_A with the introduction of grain boundaries in α-6T stems from the presence of submicrometer voids between grains. Whereas solution processing TES ADT results in a continuous film, physical crevices are absent at the boundaries where two growing spherulites impinge.[17]

On the other hand, we can also compare our results against the E_A for charge transport in polymer semiconductors. Temperature-dependent measurements on OFETs fabricated with directionally crystallized thin films of poly(3-hexylthiophene), P3HT, resulted in an E_A of 60–80 meV across LA boundaries and 70–100 meV across HA boundaries.[4c] This muted impact of the boundary on E_A relative to that reported for α-6T can be attributed to the presence of polymer chains bridging neighboring crystallites, thereby reducing the energy barrier to intercrystallite charge transport.[4c,6] The activation energies extracted for charge transport across TES ADT spherulites are more comparable to those reported for charge transport across P3HT crystallites than they are for charge transport across α-6T grains. We believe this similarity between TES ADT and P3HT—despite TES ADT being a molecular semiconductor and P3HT a polymer—stems from connectivity between their crystalline superstructures. Given that TES ADT is deposited as a continuous thin film after which crystallization takes place upon solvent-vapor annealing, ISBs formed as a consequence of two impinging spherulites are crevice-free and likely to contain pinned molecules. Akin to polymer chains providing connectivity between neighboring crystallites,[4c,6] we thus believe these molecules can serve to electronically bridge neighboring spherulites in TES ADT thin films, effectively reducing the impact of ISBs on charge transport. While obtaining physical evidence for the presence of pinned TES ADT at ISBs is challenging, we are nonetheless gratified to see a recent transient absorption microscopy study providing a picture that is consistent with our hypothesis. As opposed to a molecularly sharp interface, Wong and co-workers observed the presence of nanoscale crystalline domains whose orientations are different from those of the impinging grains in drop-cast triisopropylpentacene.[18] Although they did not probe the electrical characteristics of these boundaries, they surmised that the presence of these nanocrystalline domains—as opposed to having a clean interface—will negatively impact intergrain charge transport. However, pristine and molecularly sharp intergrain boundaries almost never exist because they often contain nanoscopic voids. Our comparison indicates that the presence of pinned molecules at the boundary is more favorable for charge transport compared to pristine interfaces in the presence of intergrain voids. Not unlike how polymer chains electrically connect neighboring crystallites in polymer semiconductor thin films, pinned TES ADT at ISBs facilitates charge transport from one spherulite to another. A similar observation was made in thin-film transistors comprising blends of 2,8-difluoro-5,11-triethylsilylethynyl anthradithiophene (diF-TES ADT):poly(triarylamine) (PTAA), in which the authors reported substantially less resistive grain boundaries and speculated PTAA's role in connecting neighboring diF-TES ADT grains.[4d]

To further illustrate the impact of the ISBs, we can measure the energy barrier to charge transport as a function of V_G.[3a,15] In this rearrangement of Equation (2), we hold T constant at 295 K and sweep V_G; since μ_{eff} is now calculated as devices are turning from off to on, we swap E_A for the more general Δ:

$$\Delta = kT\ \ln\left(\mu_0/\mu_{eff}\left(V_G - V_T\right)|_T\right) \tag{3}$$

For μ_0, we use the values calculated from the T-dependent measurements. As shown in **Figure 4**, once the devices are fully on, Δ plateaus to the corresponding E_A reported above for each type of device. The fact that Δ is independent of V_G where $V_G - V_T < 0$ indicates that the assumption of a single trap level at E_A is appropriate; a distribution broader than the assumed exponential distribution of trap states would have caused Δ to continue to vary with V_G in this regime. In contrast, the Δ of

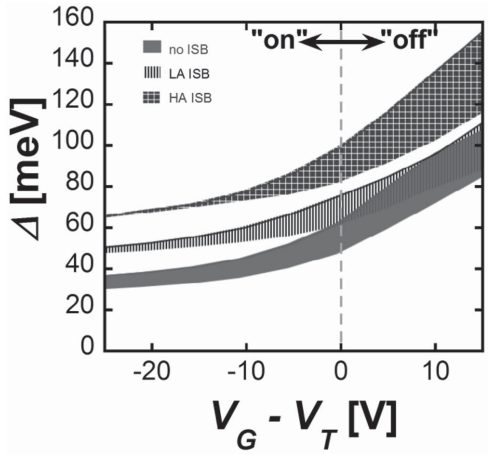

Figure 4. The energy barrier to charge transport, Δ, calculated as a function of $V_G - V_T$ using Equation (3) within a single spherulite (solid), across an LA ISB (stripes), and across an HA ISB (crosshatch). Bands represent the spread in Δ (± one standard deviation) across three to four devices. The Δ for devices comprising a single spherulite and an LA ISB overlap extensively at positive $V_G - V_T$, but plateau to the values corresponding to the E_A for each case once the devices are fully turned on.

α-6T is shown to be quite sensitive to the V_G in its fully on state,[3a] indicating that, in addition to being much deeper, its trap distribution is also much broader than that in TES ADT. Comparing the gate dependence of Δ across the three devices reveals that charge transport is characteristically different in these devices. Looking first between the devices constructed within a single spherulite and across an LA ISB, we observe that the presence of an LA ISB adds ≈15 meV energy barrier to charge transport when the devices are in their fully on states. Before the devices are fully on, however, the gate dependence of Δ is comparable, suggesting trap filling is comparable in these devices. In contrast, when comparing between devices constructed within a single spherulite and across an HA ISB, the HA ISB adds an additional ≈30 meV energy barrier to charge transport in devices across the entire range of applied voltages. Thus, the additional energy barrier due to the HA ISB in the voltage regime where the device is turning on, related to the additional trap states that must be filled, is as significant as the additional energy barrier in the voltage regime where the devices are fully on, related to the higher E_A to charge transport.

Having established the energy level of traps within TES ADT spherulites and across ISBs, we turn our attention to quantifying the density of these traps. To do so, we calculate the subthreshold swing (SS) from the gated two-probe V_G-drain current (I_D) curves measured across the devices in each case[11,19]

$$SS = \left[\frac{d\log(I_D)}{dV_G}\right]^{-1} \quad (4)$$

For devices constructed within an individual spherulite or those spanning individual LA ISBs, SS = 1.8 ± 0.7 V decade^{-1}, while devices spanning HA ISBs exhibit SS = 4 ± 1 V decade^{-1}. From the SS, we can estimate the maximum density of shallow traps per electronvolt, $N_{SS,max}$:[11]

$$N_{SS,max} = \left[\frac{SS\ \log(e)}{kT/q} - 1\right]\frac{C_{ox}}{q^2} \quad (5)$$

We can thus estimate the density of shallow traps, N_T, at the trap level by multiplying $N_{ss,max}$ by E_A. We find $N_T = 0.7 \times 10^{11}$ cm^{-2} for the devices whose channel is within a spherulite and whose channel spans an LA ISB, and $N_T = 2.7 \times 10^{11}$ cm^{-2} for the device whose channel spans an HA ISB. As mentioned previously, the boundaries within a spherulite are also "low-angle" in nature, so it is reasonable that devices with channels within a spherulite or across an LA ISB exhibit comparable densities of traps. In contrast, the high angle of mismatch at the HA ISB generates an additional 2.0×10^{11} shallow traps cm^{-2} compared to LA inter- or intraspherulite boundaries. Our calculation assumes that the shallow traps whose density we calculated with the SS are the same shallow traps whose energy level we calculated with the low-temperature mobility measurements. The E_A values we measured from fully-on devices likely represent the energy level of the very shallowest of traps. In contrast, the SS is measured while the device is turning on, so the calculated N_Ts likely include traps at slightly deeper energy levels. Thus, any discrepancy between these parameters may not allow us to observe an increase in N_T due to an LA ISB, as we might expect to find. However, Figure 4 shows that the gate dependence of Δ is comparable across multiple single-spherulite and LA ISB devices, which lends additional support to our observation of similar trap densities in these devices. Finally, it is interesting to note that the shallow trap densities in our solution-grown crystalline TES ADT films are comparable to those estimated by a completely different method in OFETs based on vapor-grown tetracene single crystals that exhibit comparable mobilities and similar activation energies.[20]

In summary, we have established that boundaries impose two distinct bottlenecks to charge transport that can be quantified by the energy level and density of shallow traps. Put simply, our results indicate that, even after the additional trap states at the ISB are filled, the angle of mismatch of the ISB continues to affect charge transport across the film. Although Rivnay and co-workers previously suggested that the angle of mismatch would affect the resistance of the boundary,[21] they were not able to decouple the impact of the grain boundaries from the intrinsic charge transport anisotropy of the organic semiconductor in their study. Since TES ADT spherulites do not exhibit any charge transport anisotropy,[8] we are able to fully isolate and quantify the impact of the ISBs on charge transport across the film. Our results thus reveal that additional trap states at the boundary are not the sole barrier to charge transport. In fact, the presence of LA ISBs does not result in more traps compared to the presence of LA intraspherulite boundaries; only HA ISBs introduce additional shallow traps due to the more significant misorientation of molecular angles at the boundary. Instead, the additional barrier to charge transport across the boundary is caused by the higher trap energies at the LA and HA ISBs compared to the LA intraspherulite boundaries.

3. Conclusions

TES ADT's ISBs qualitatively affect charge transport in the following ways. The shallow trap density contributes to the

voltage-dependent barrier to charge transport, since these traps must be filled by additional gate-induced charges. These shallow traps can be evidenced by an increase in SS. Additionally, a higher activation energy is needed to push charges through these misoriented pathways. This energy demand is reflected in the depth of the shallow trap level, contributing to the voltage-independent barrier to charge transport.

As previously hypothesized,[17] the impact of boundaries can depend on the film processing method during which they are formed. With the addition of a boundary, E_A increases from 34 up to 66 meV for our solution-processed TES ADT devices, while E_A increases from 40 to over 200 meV for thermally evaporated α-6T. Even though the interfaces between α-6T's thermally evaporated grains are "neat and clean" (i.e., molecularly sharp), they include crevices which greatly increase the resistance to charge transport between grains. In contrast, TES ADT's ISBs likely include molecules pinned between the impinging spherulites, which facilitate charge transport over the boundary. Thus, even though TES ADT is a molecular semiconductor, its ISBs are more similar to the boundaries between crystallites in polymer semiconductor films.

TES ADT's unique crystallization behavior thus provides the best characteristics of both polymeric and molecular semiconductors. We routinely obtain highly crystalline films with spherulites that appear to be electrically connected through the presence of pinned molecules at ISBs. However, TES ADT's ISBs are, stochastically primarily HA in nature, and as our work has shown, this angle of mismatch affects charge transport through both the density and energy level of traps. These results highlight the importance of reducing both the number of domain boundaries and their angle of molecular mismatch within device channels in order to maximize charge transport.

4. Experimental Section

Film Formation: TES ADT was synthesized according to previously published procedures.[22] Solutions of TES ADT were prepared by dissolving TES ADT in toluene at a concentration of 2 wt%. Since TES ADT readily photobleaches,[17] solutions were used within 4 min of preparation. 300 nm thick thermally grown SiO_2 on highly doped-Si wafers purchased from Process Specialties was consecutively sonicated in acetone, isopropyl alcohol, and deionized water and then dried with house nitrogen. Thin films (100 nm thick) of TES ADT were formed on these substrates by spin coating the solution at 1000 RPM for 60 s. The substrates were subsequently annealed at 90 °C for 2 min on a hot plate to remove residual solvent from the film. Solvent-vapor annealing induced macroscopic crystallization of the TES ADT thin film. A solvent-vapor annealing chamber was used to expose the samples to 0.019 vol% 1,2-dichloroethane vapor in a N_2 carrier gas; the details of this setup are described in ref. [23].

Transistor Fabrication: Transistors were fabricated with active channels comprising a single LA or HA ISB. The selected active areas were electrically isolated from those of neighboring transistors by removing the surrounding TES ADT film. Top-contact electrodes were deposited onto TES ADT thin films by thermally evaporating 100 nm thick Au through a shadow mask that had been meticulously aligned so that the ISB traversed the length of the inner two electrodes. The samples were coated with a 2 μm thick parylene layer by chemical-vapor deposition in a tube furnace to increase their mechanical stability on thermal cycling; the details of this setup are described in ref. [24]. As a control, devices were also prepared with active channels residing entirely on a single spherulite (containing LA intraspherulite boundaries but no ISBs) to quantify the intraspherulite electrical characteristics of TES ADT.

Gated Four-Probe Measurements: Gated four-probe measurements were conducted in a cryogenic Lakeshore probe station using an Agilent 4145B semiconductor parameter analyzer by flowing current through the outer two electrodes and measuring the voltage drop across the inner two electrodes, in the presence of a gate bias. The capacitance of the 300 nm thick SiO_2 dielectric layer is 1.06×10^{-8} F cm^{-2}. For four-probe measurements, the channel length and width were 0.2 and 0.1 mm, respectively. For two probe measurements, the channel length and width were 0.8 and 1.5 mm, respectively. Low temperature measurements were performed in the dark at 10^{-6} Torr on a sample stage chilled with a constant flow of liquid nitrogen.

Supporting Information

Supporting Information is available from the Wiley Online Library or from the author.

Acknowledgements

Y.-L.L. acknowledges support from the National Science Foundation (NSF) Materials Research Science and Engineering Centers program through the Princeton Center for Complex Materials (DMR-1420541) and the Photovoltaics Program at the Office of Naval Research (N00014-11-10328). J.E.A. and M.M.P. thank the NSF (CMMI-1255494) for support of organic semiconductor synthesis. A.K.H. was supported by an NSF Graduate Research Fellowship.
Note: Equation 2 was corrected on September 16, 2015.

Received: April 24, 2015
Revised: July 1, 2015
Published online: August 12, 2015

[1] a) G. Nan, Z. Li, *Org. Electron.* **2011**, *12*, 2198; b) M. Mladenović, N. Vukmirović, I. Stanković, *J. Phys. Chem. C* **2013**, *117*, 15741; c) S. Mansouri, S. Zorai, R. Bourguiga, *Synth. Met.* **2012**, *162*, 231; d) A. Di Carlo, F. Piacenza, A. Bolognesi, B. Stadlober, H. Maresch, *Appl. Phys. Lett.* **2005**, *86*, 263501; e) L. G. Kaake, P. F. Barbara, X.-Y. Zhu, *J. Phys. Chem. Lett.* **2010**, *1*, 628.

[2] a) D. Knipp, R. A. Street, A. R. Volkel, *Appl. Phys. Lett.* **2003**, *82*, 3907; b) S. D. Wang, T. Miyadera, T. Minari, Y. Aoyagi, K. Tsukagoshi, *Appl. Phys. Lett.* **2008**, *93*, 043311.

[3] a) A. B. Chwang, C. D. Frisbie, *J. Appl. Phys.* **2001**, *90*, 1342; b) T. W. Kelley, C. D. Frisbie, *J. Phys. Chem. B* **2001**, *105*, 4538; c) G. Horowitz, M. E. Hajlaoui, *Synth. Met.* **2001**, *122*, 185; d) H. Yang, T. J. Shin, M.-M. Ling, K. Cho, C. Y. Ryu, Z. Bao, *J. Am. Chem. Soc.* **2005**, *127*, 11542; e) R. L. Headrick, S. Wo, F. Sansoz, J. E. Anthony, *Appl. Phys. Lett.* **2008**, *92*, 063302; f) J. Chen, C. K. Tee, M. Shtein, J. E. Anthony, D. C. Martin, *J. Appl. Phys.* **2008**, *103*, 114513; g) R. Li, J. W. Ward, D.-M. Smilgies, M. M. Payne, J. E. Anthony, O. D. Jurchescu, A. Amassian, *Adv. Mater.* **2012**, *24*, 5553; h) M. Nakamura, H. Ohguri, N. Goto, H. Tomii, M. Xu, T. Miyamoto, R. Matsubara, N. Ohashi, M. Sakai, K. Kudo, *Appl. Phys. A: Mater. Sci. Process.* **2008**, *95*, 73.

[4] a) R. J. Chesterfield, J. C. McKeen, C. R. Newman, P. C. Ewbank, D. A. da Silva Filho, J.-L. Bredas, L. L. Miller, K. R. Mann, C. D. Frisbie, *J. Phys. Chem. B* **2004**, *108*, 19281; b) M. Shtein, J. Mapel, J. B. Benziger, S. R. Forrest, *Appl. Phys. Lett.* **2002**, *81*, 268; c) L. H. Jimison, M. F. Toney, I. McCulloch, M. Heeney, A. Salleo, *Adv. Mater.* **2009**, *21*, 1568; d) S. Hunter, T. D. Anthopoulos, *Adv. Mater.* **2013**, *25*, 4320.

[5] F. J. Meyer zu Heringdorf, M. C. Reuter, R. M. Tromp, *Nature* **2001**, *412*, 517.

[6] a) R. Street, J. Northrup, A. Salleo, *Phys. Rev. B* **2005**, *71*, 165202; b) R. Noriega, J. Rivnay, K. Vandewal, F. P. V. Koch, N. Stingelin, P. Smith, M. F. Toney, A. Salleo, *Nat. Mater.* **2013**, *12*, 1038.

[7] A. G. Shtukenberg, Y. O. Punin, E. Gunn, B. Kahr, *Chem. Rev.* **2012**, *112*, 1805.
[8] S. S. Lee, M. A. Loth, J. E. Anthony, Y.-L. Loo, *J. Am. Chem. Soc.* **2012**, *134*, 5436.
[9] G. S. Was, S. M. Bruemmer, *Mater. Sci. Forum* **1989**, *46*, 237.
[10] a) V. Podzorov, in *Organic Field-Effect Transistors* (Eds: Z. Bao, J. Locklin), CRC Press, Boca Raton, FL **2007**, pp. 27–72; b) V. Coropceanu, J. Comil, D. A. da Silva Filho, Y. Olivier, R. Silbey, J.-L. Bredas, *Chem. Rev.* **2007**, *107*, 926.
[11] J. A. Letizia, J. Rivnay, A. Facchetti, M. A. Ratner, T. J. Marks, *Adv. Funct. Mater.* **2010**, *20*, 50.
[12] a) A. B. Kaiser, *Rep. Prog. Phys.* **2001**, *64*, 1; b) P. Stallinga, *Electrical Characterization of Organic Electronic Materials and Devices*, John Wiley & Sons, Chichester, UK **2009**.
[13] P. V. Pesavento, K. P. Puntambekar, C. D. Frisbie, J. C. McKeen, P. P. Ruden, *J. Appl. Phys.* **2006**, *99*, 094504.
[14] I. N. Hulea, S. Fratini, H. Xie, C. L. Mulder, N. N. Iossad, G. Rastelli, S. Ciuchi, A. F. Morpurgo, *Nat. Mater.* **2006**, *5*, 982.
[15] A. B. Chwang, C. D. Frisbie, *J. Phys. Chem. B* **2000**, *104*, 12202.
[16] a) I. G. Lezama, A. F. Morpurgo, *MRS Bull.* **2013**, *38*, 51; b) M. Mas-Torrent, C. Rovira, *Chem. Rev.* **2011**, *111*, 4833; c) P. J. Skabara, J.-B. Arlin, Y. H. Geerts, *Adv. Mater.* **2013**, *25*, 1948.
[17] S. S. Lee, J. M. Mativetsky, M. A. Loth, J. E. Anthony, Y.-L. Loo, *ACS Nano* **2012**, *6*, 9879.
[18] C. Y. Wong, B. L. Cotts, H. Wu, N. S. Ginsberg, *Nat. Commun.* **2015**, *6*, 5946.
[19] a) V. Podzorov, *MRS Bull.* **2013**, *38*, 15; b) C. Li, L. Duan, H. Li, Y. Qiu, *J. Phys. Chem. C* **2014**, *118*, 10651.
[20] M. F. Calhoun, C. Hsieh, V. Podzorov, *Phys. Rev. Lett.* **2007**, *98*, 096402.
[21] J. Rivnay, L. H. Jimison, J. E. Northrup, M. F. Toney, R. Noriega, S. Lu, T. J. Marks, A. Facchetti, A. Salleo, *Nat. Mater.* **2009**, *8*, 952.
[22] M. M. Payne, S. A. Odom, S. R. Parkin, J. E. Anthony, *Org. Electron.* **2004**, *6*, 3325.
[23] S. S. Lee, S. B. Tang, D.-M. Smilgies, A. R. Woll, M. A. Loth, J. M. Mativetsky, J. E. Anthony, Y.-L. Loo, *Adv. Mater.* **2012**, *24*, 2692.
[24] V. Podzorov, V. M. Pudalov, M. E. Gershenson, *Appl. Phys. Lett.* **2003**, *82*, 1739.